AAS 15-237

OPTIMIZATION OF MANY-REVOLUTION, ELECTRIC-PROPULSION TRAJECTORIES WITH ENGINE SHUTOFF CONSTRAINTS

Jason A. Reiter,[*] Austin K. Nicholas,[†] and David B. Spencer[‡]

Many-revolution, solar-electric-propulsion trajectories are difficult to computationally optimize. One of the most significant, unsolved problems with optimizing low-orbit trajectories using feedback control is eclipse constraints. Employing a new forward-looking feedback control technique, however, allows for an optimization of the trajectory including the effects of eclipses or any other arbitrary engine shutoff periods. The control law applies weightings to the optimal thrusting angles based on the spacecraft's relative instantaneous efficiency over one revolution, which includes the effect of the engine shutoffs. This method also facilitates simple exploration of the propellant versus time trade space in the presence of engine shutoff constraints.

INTRODUCTION AND BACKGROUND

Many techniques exist for solving electric propulsion trajectories, including Q-law, nonlinear programming, indirect optimization, optimal control, and feedback control. Though Q-law, nonlinear programming, and indirect optimization can provide highly optimal propellant versus time curves, the nature of these techniques only allows for eclipse periods to be incorporated as unplanned shutoffs.[1] While optimal control can account for eclipse periods and other arbitrary engine shutoff periods, only the time optimal solution can be found with this method.[2] Feedback control, however, allows for an optimization of the trajectory including the effects of shutoff periods while creating a complete propellant versus time curve.

With techniques that can't optimize for shutoff constraints, eclipse periods are accounted for simply as unplanned shutoffs. When creating a propellant versus time curve, propellant use is lowered by taking more time and only thrusting when it is most efficient to do so. If an unplanned shutoff were to occur during the small amount of time planned for thrusting, this would mean a large increase in flight time, if the transfer converges at all. This new forward-looking feedback control allows for the trajectory to be optimized while taking eclipses and other shutoff periods into account. This helps to avoid any convergence and time of flight issues. If the eclipse period occurs when it is most efficient to thrust, then the technique allows for thrusting at slightly less

[*] Graduate Student, Department of Aerospace Engineering, The Pennsylvania State University, 229 Hammond Building, University Park, PA 16802.
[†] Systems Engineer, Jet Propulsion Laboratory, California Institute of Technology, 4800 Oak Grove Drive, M/S 301-165, Pasadena, CA 91109.
[‡] Professor, Department of Aerospace Engineering, The Pennsylvania State University, 229 Hammond Building, University Park, PA 16802.

efficient points to ensure that the transfer is still completed in a realistic time frame. This new technique means much more realistic time of flight and fuel use estimates for solar powered low-thrust transfers and may prove useful in applying similar methods to future tools.

METHODOLOGY

The main concept behind this technique is the use of feedback control. With an initial state and desired end state, the optimal thrusting angle can be calculated throughout the trajectory to reach the desired end state. Applying directionality and efficiency thresholds also allows for an increase in propellant usage efficiency at the expense of a longer flight time.

Approach

In reference 3, a feedback control law is described in which the optimal angle to increase each classical orbital element (COE) is weighted based on the COEs relative distance from its end state. The weighted angles are then combined so that the spacecraft is thrusting in the optimal direction for all desired COEs to reach their end states. A threshold is then applied so that thrusting does not occur at points where it is inefficient to do so.

Using this control law as a basis, changes are made to increase the optimality of the tool. In addition to the location based weighting, a second weighting is applied to the angle from the maneuver efficiency. An additional threshold is also applied to account for conflicting optimal thrusting directions. The optimal thrusting angle is updated at each time step and the efficiency and thrusting direction are compared to the designated cut-off thresholds. If the thresholds are not met, thrusting does not occur. Applying various efficiency thresholds allows for a curve to be constructed comparing fuel mass use and maneuver time.

Propagation Method

While ordinary differential equation solvers, like MATLAB's ode45, are commonly used for propagating orbital states, to save computation time and avoid convergence tolerance issues, the COE differential equations presented in [1] are combined with Euler's method to propagate the orbital states. The differential equations for the semimajor axis, eccentricity, inclination, right ascension of the ascending node, and argument of perigee are

$$\frac{da}{dt} = \frac{2a^2}{h} \left|\vec{f}\right| cos\beta \left\{e\, sin\nu\, sin\alpha + \frac{p}{r}\, cos\alpha\right\} \tag{1}$$

$$\frac{de}{dt} = \frac{1}{h} \left|\vec{f}\right| cos\beta \left\{p\, sin\nu\, sin\alpha + \left((p+r)\, cos\nu + re\right) cos\alpha\right\} \tag{2}$$

$$\frac{di}{dt} = \left|\vec{f}\right| \frac{r}{h}\, cosu\, sin\beta \tag{3}$$

$$\frac{d\Omega}{dt} = \left|\vec{f}\right| \frac{r}{h} \frac{sinu}{sini}\, sin\beta \tag{4}$$

$$\frac{d\omega}{dt} = \frac{1}{he} \left|\vec{f}\right| cos\beta \left\{-p\, cos\nu\, sin\alpha + (p+r)\, sin\nu\, cos\alpha\right\} - \left|\vec{f}\right| \frac{r\, sinu\, cosi}{h\, sini}\, sin\beta \tag{5}$$

where h is the angular momentum [in kg*m^2/s], $\vec{f}$ is the acceleration vector exerted by the thruster on the spacecraft [in m/s^2], β is the out-of-plane thrusting angle, e is the eccentricity, ν is the true anomaly, α is the in-plane thrusting angle, p is the semilatus rectum [in km], r is the distance from the spacecraft to the center of the central body [in km], u is the true latitude, and i is the inclination. All angles are expressed in radians.

The Control Law

The angles, α and β, in the equations above are solved for each COE separately. These are the optimal in-plane (α) and out-of-plane (β) thrusting angles for the maximum instantaneous change of each orbital element, regardless of their effect on the other orbital elements. With α, the in-plane angle and β, the out-of-plane angle, the equations can be summarized in Table 1 (originally from Reference 3 and repeated here for clarity).

Table 1. Optimal in-plane (α) and out-of-plane (β) thrust angles for the maximum instantaneous change of each orbital element.[3]

	Thrusting Angles	
Semi-major axis (a)	$\alpha = \tan^{-1}\left(\frac{e\sin\nu}{1+e\cos\nu}\right)$	$\beta = 0$
Eccentricity (e)	$\alpha = \tan^{-1}\left(\frac{\sin\nu}{\cos\nu+\cos E}\right)$	$\beta = 0$
Inclination (i)	$\alpha = 0$	$\beta = sgn(\cos(\omega+\nu))\frac{\pi}{2}$
RAAN (Ω)	$\alpha = 0$	$\beta = sgn(\sin(\omega+\nu))\frac{\pi}{2}$
Argument of Perigee (ω)	$\alpha = \tan^{-1}\left(\frac{1+e\cos\nu}{2+e\cos\nu}\cot\nu\right)$	$\beta = \tan^{-1}\left(\frac{e\cot i\sin(\omega+\nu)}{\sin(\alpha-\nu)\,(1+ecos(\nu)-\cos(\alpha)\sin(\nu)}\right)$

When more than one COE is changed in the orbital maneuver, the control law is used to combine the separate angles to make one optimal thrusting angle vector. To do this, the angles must first be transformed into the body-fixed RCN (radial-circumferential-normal) reference frame. This reference is such that the radial component is aligned with the radial unit vector positive in the zenith direction, the normal component is aligned with the osculating angular momentum vector positive in the direction of the cross product $\vec{R}x\vec{V}$ and the circumferential component is normal to the radius vector in the orbital plane and completes the right-handed triad of unit vectors, as seen in Figure 1 left. Using Figure 1 right as reference, the transformation from α and β to RCN can be calculated for each COE.

$$\vec{T}_{COE} = [\sin(\alpha)\cos(\beta), \cos(\alpha)\cos(\beta), \sin(\beta)]^T \tag{6}$$

To this vector, two weightings are applied. The first is based on the relative value for the COE compared to its starting state and desired final state,

$$w_{position} = \frac{COE_1 - COE}{|COE_1 - COE_0|} \tag{7}$$

where COE_1 is the desired final value, COE is the instantaneous osculating value, and COE_0 is the starting value for each COE being controlled. The second weighting is calculated using the instantaneous maneuver efficiency of each COE. As expected, the efficiency to change the satellites position varies throughout an orbit. Table 2 summarizes the locations (true anomaly) of the maximum instantaneous efficiency for each COE and the equations for the instantaneous efficiency at any true anomaly value.

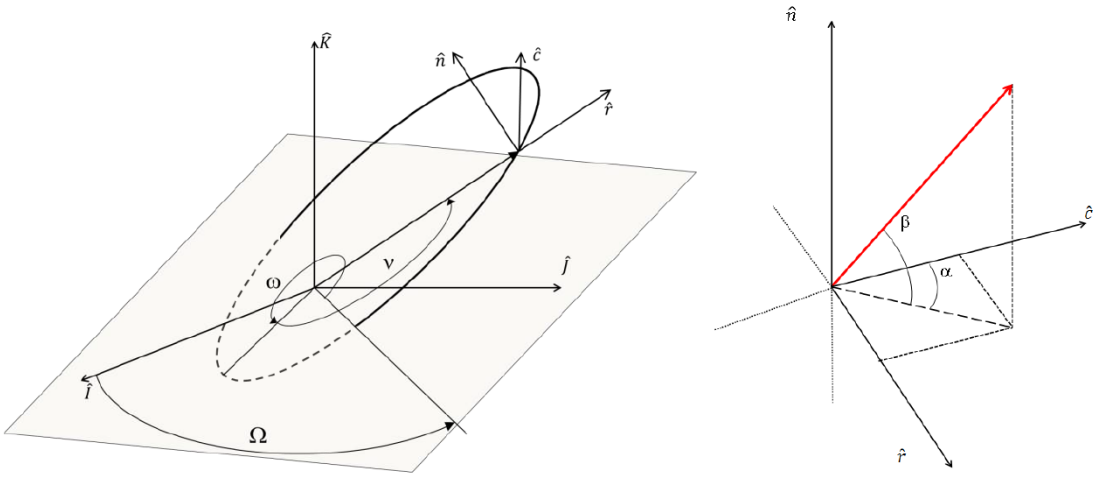

Figure 1. Left: RCN reference frame with respect to the Central-Body-Centered inertial reference frame (IJK).
Right: α and β thrust angles with respect to the RCN reference frame.[3]

Table 2. Point of the orbit providing the maximum rate of change and the expression of the maneuver efficiency, η, for each considered COE.[3]

COE	ν_{max}	η
a	$\nu_a = 0$	$\eta_a = \lvert\vec{V}\rvert\sqrt{\frac{a}{\mu}\frac{1-e}{1+e}}$
e	$\nu_e = \pi$	$\eta_e = \frac{1}{2}\frac{1+2ecos(\nu)+cos^2\nu}{1+ecos(\nu)}$
i	$\sin(\nu_i+\omega) = -esin(\omega)$	$\eta_i = \frac{\lvert\cos(\omega+\nu)\rvert}{1+ecos\nu}\left(\sqrt{1-e^2sin^2\omega} - e\lvert cos\omega\rvert\right)$
Ω	$\cos(\nu_\Omega+\omega) = -ecos(\omega)$	$\eta_\Omega = \frac{\lvert\sin(\omega+\nu)\rvert}{1+ecos\nu}\left(\sqrt{1-e^2cos^2\omega} - e\lvert sin\omega\rvert\right)$
ω	$\cos\nu_\omega = \left[\frac{1-e^2}{e^3}+\sqrt{\frac{1}{4}\left(\frac{1-e^2}{e^3}\right)}+\frac{1}{27}\right]^{\frac{1}{3}} - \left[-\frac{1-e^2}{e^3}+\sqrt{\frac{1}{4}\left(\frac{1-e^2}{e^3}\right)}+\frac{1}{27}\right]^{\frac{1}{3}} - \frac{1}{e}$	$\eta_\omega = \frac{1}{4}\frac{1+sin^2\nu}{1+ecos\nu}\frac{1+ecos\nu_{\omega max}}{1+sin^2\nu_{\omega max}}$

Using the equations for instantaneous maneuver efficiency, η, the second weighting is found by dividing the instantaneous efficiency for the COE by the average maneuver efficiency for that COE over one orbit.

$$w_{eff} = \frac{\eta_{COE}}{\int_0^{2\pi} \eta_{COE}(\nu) d\nu} \tag{8}$$

The two weights are then multiplied by the optimal thrusting vector for each COE and the resulting vectors for all controlled COEs are added together to get the optimal instantaneous thrusting angle,

$$\vec{T} = \sum_{COE} w_{eff}\, w_{position}\, \vec{T}_{COE} \tag{9}$$

where Σ_{COE} signifies the summation of the term for all controlled COEs. This vector is then transformed back into angles α and β using Eqs. 10 and 11, which are inserted into Eqs. 1-5 to propagate the transfer at each time step.

$$\alpha = atan2\left(\frac{\vec{T}_R}{\vec{T}_C}\right) \tag{10}$$

$$\beta = atan2\left(\frac{\vec{T}_N}{\sqrt{\vec{T}_R{}^2 + \vec{T}_C{}^2}}\right) \tag{11}$$

In Eqs. 10 and 11, *atan2* is the arctangent function with two arguments to return the angle in the correct quadrant.

Applying Cut-Off Thresholds

With the control law and propagation method in place, it is possible to get converging solutions to the desired orbit transfers. However, the optimality at this point is lacking. Applying two cut-off thresholds improves the optimality of the tool by a great deal. The first threshold is based on maneuver efficiency. As mentioned previously, the instantaneous maneuver efficiency varies over an orbit. The technique allows a cutoff based on instantaneous maneuver efficiency to be implemented in two different methods. The first method, as demonstrated in reference 3, is an independent efficiency threshold, where the instantaneous maneuver efficiencies for each COE are averaged and compared to a threshold (in percent) provided by the user. However, this method does not take into account the range of possible maneuver efficiency values. If, for example, the average efficiency ranges between 70 and 90%, then cut-off values of 70% and lower would do nothing to improve the results and the user would have to have prior knowledge of the trajectory to know this.

The second method improves on this by using a dependent efficiency threshold. Using this method, the instantaneous efficiency for each COE is weighted by the average efficiency for the COE for one orbit, like the weighting system described previously. These weightings for each COE are summed together and divided by the total number of COEs being controlled and is then compared to an input threshold adjusted using a cumulative distribution function for the instantaneous efficiencies over one orbit.

$$\frac{\sum_{COE} \frac{\eta_{COE}}{\int_0^{2\pi} \eta_{COE}(\nu) d\nu}}{Number\ of\ COEs\ Controlled} < Adjusted\ Threshold \tag{12}$$

Using the weighting system combined with the cumulative distribution function means that, no matter what cut-off value the user inputs, it will cut-off the inefficient parts of the trajectory. The cumulative distribution function was chosen to produce more meaningful results. For exam-

ple, if a cut-off threshold of 60% is inputted, then thrusting will only occur in the most efficient 40% of the orbit. While either of these two methods can be used, the latter is recommended for more meaningful results.

This threshold method is also extremely versatile. Since the instantaneous value compared to the threshold is dependent on the average efficiency of the orbit, the value can be adjusted for any possible periods where thrusting is prohibited. Adding eclipse constraints and pointing requirements is straightforward, and is reflected in the threshold calculation. If, for example, an eclipse occurred at the point of the orbit where it is very efficient to thrust, the average maneuver efficiency value would be lower, and therefore locations with lower instantaneous efficiency values would be weighted more heavily, and chosen to meet the input threshold.

The second cut-off threshold is based on directionality. For certain orbital maneuvers, the combination of COEs being adjusted means that, at times, they will conflict in their optimal thrusting directions. When the conflict occurs, the resulting thrusting vector will not be ideal for reaching the desired final state because it harms one element at the expense of helping another. To avoid this, a threshold is applied to ensure that thrusting only occurs when it is ideal to do so. The directionality value is found from the instantaneous weighted thrusting angle for each COE by normalizing the total of all angle vectors and dividing that by the sum of each angle vector normalized.

$$\frac{\|\sum_i \vec{T}\|}{\sum_i \|\vec{T}\|} < directionality \tag{13}$$

This results in a value between zero and one. Unlike the efficiency threshold, however, choosing a directionality threshold value is not straight-forward. The optimal directionality threshold varies from case to case and, in some cases, there is such thing as a bad input. For example, if the threshold is set above 0.7071 (as seen in Figure 2), thrusting for perpendicular vectors of equal length cannot occur. This means that, for instance, it would be impossible to increase both inclination and semimajor axis/eccentricity and the same time. However, if only in-plane thrusting is required, this would not be an issue.

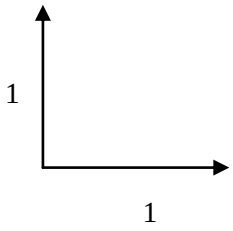

$$\frac{\|[0,1]+[1,0]\|}{\|[0,1]\|+\|[1,0]\|} = \frac{\sqrt{2}}{2} = 0.7071$$

Figure 2. The directionality value for thrusting for perpendicular vectors.

The same method can be applied to show how the directionality threshold serves its purpose. If two COEs require thrusting in opposite directions, the directionality becomes small and easily caught by a cut-off threshold, as seen in Figure 3.

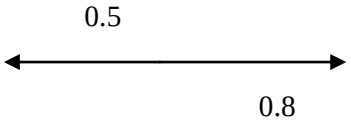

$$\frac{\|[0.8,0]+[-0.5,0]\|}{\|[0.8,0]\|+\|[-0.5,0]\|} = 0.2308$$

Figure 3. The directionality value for vectors in opposite directions.

TECHNIQUE VERIFICATION

As mentioned earlier, a variety of techniques, such as Q-law, nonlinear programming, and indirect optimization, have been explored for solving electric propulsion orbit transfers. A comparison of these techniques was made in reference 1 and their results were presented.

Test Cases

Running a feedback control tool employing the above technique for these same cases provides a great basis for comparison and can highlight the capabilities and limitations of the tool. Out of the cases shown in Table 3, all but Case D will be compared graphically below.

Table 3. Test cases for various COE changes and engine properties[1]

Case	Orbit	a, km	e	i, deg.	ω, deg	Ω, deg	Thrust, N	Initial Mass, kg	Specific Impulse, s	Central Body
A	Init.	7000	0.01	0.05	0	0	1	300	3100	Earth
	Targ.	42000	0.01	free	free	free				
B	Init.	24505.9	0.725	7.05	0	0	0.350	2000	2000	Earth
	Targ.	42165	0.001	0.05	free	free				
C	Init.	9222.7	0.2	0.573	0	0	9.3	300	3100	Earth
	Targ.	30000	0.7	free	free	free				
D	Init.	944.64	0.015	90.06	156.90	-24.60	0.045	950	3044.98	Vesta
	Targ.	401.72	0.012	90.01	free	-40.73				
E	Init.	24505.9	0.725	0.06	0	0	2	2000	2000	Earth
	Targ.	26500	0.7	116	270	180				

Results and Analysis

Plots comparing time-of-flight and fuel consumption combinations to the methods described in reference 1 for all four cases are plotted below in Figures 4-7 to serve as a basis for analysis of the optimality of the tool and the possible sources of error in the different cases.

Figure 4 shows the fuel mass consumption vs. time-of-flight curve for Case A, which is a circular to circular altitude raising maneuver. As evident in the plot, the results closely match the minimum time solutions produced by other methods but does not follow those produced by the more robust tools at higher flight times. This, unfortunately, has to do with the nature of the control law. Because it is a feedback law, the algorithm attempts to maintain circularity along the entire trajectory, which is not fuel-optimal. This means that no matter how much extra time is allotted for the maneuver, no improvement in fuel use can be made from the time-optimal case because along-track thrusting is always executed. Removing the directionality threshold doesn't improve the situation either because semimajor axis and eccentricity often optimally thrust in opposite directions. In this particular case, the method cannot reproduce fuel optimal solutions at long flight times. Luckily, in circular-to-circular cases, it is rarely beneficial to do any maneuver besides the time-optimal one (expressed as the analytic approximation, found only from the initial and final radius and the gravitational parameter of the planet). In Case A, for example, doubling the time-of-flight only improves the fuel use by 3 kg (less than 10%), which is unlikely to be desirable.

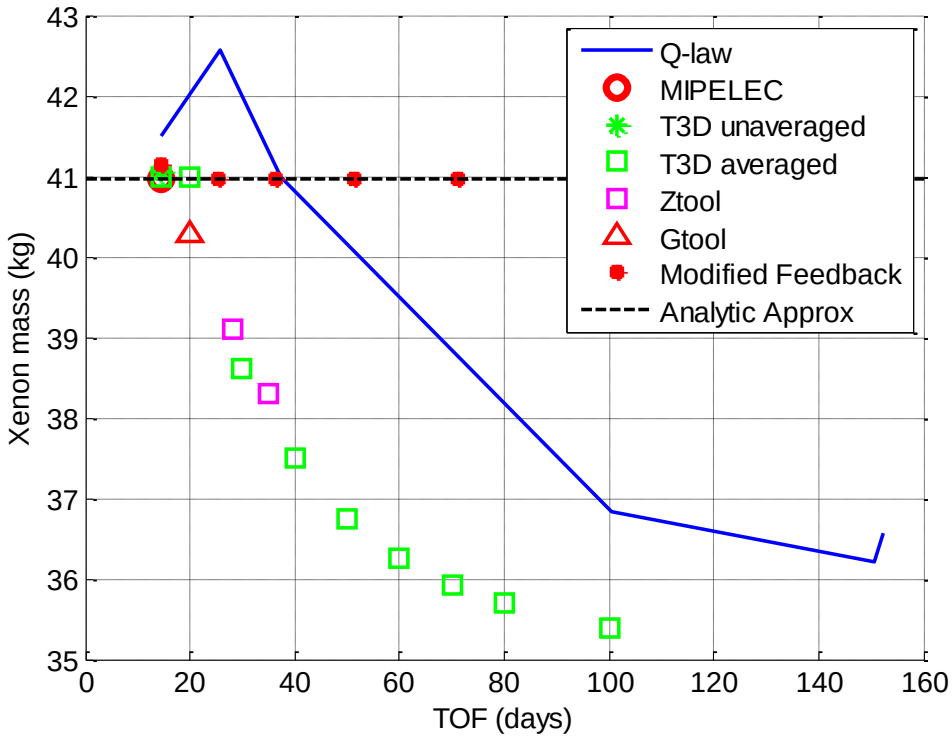

Figure 4. Fuel mass consumption vs. time-of-flight for Case A, comparing existing tools (compared in reference 1) to the modified feedback control and analytical approximation

Figure 5 shows the fuel mass consumption vs. time-of-flight curve for Case B. Since none of the COEs are being held constant, the control law performs much better and the directionality cutoff works properly to decrease both fuel use and maneuver time. With the addition of the efficiency threshold, the full fuel mass use/time-of-flight curve can be created. As evident in the plot, the tool can solve for this case with less than 5% error as compared to other methods. This amount of error is acceptable for preliminary mission design work.

The tool also performs well on Case C, as seen in Figure 6. In this case, errors are between 5% and 15%, but follow the trend of the more robust tools. Further, the fuel values predicted always err above those from the more robust tool, which is preferable for preliminary mission design. Since this case requires change in only semimajor axis and eccentricity, and the method provides both time- and fuel- optimal results, it becomes more certain that the source of error in Case A was in constraining the eccentricity to zero.

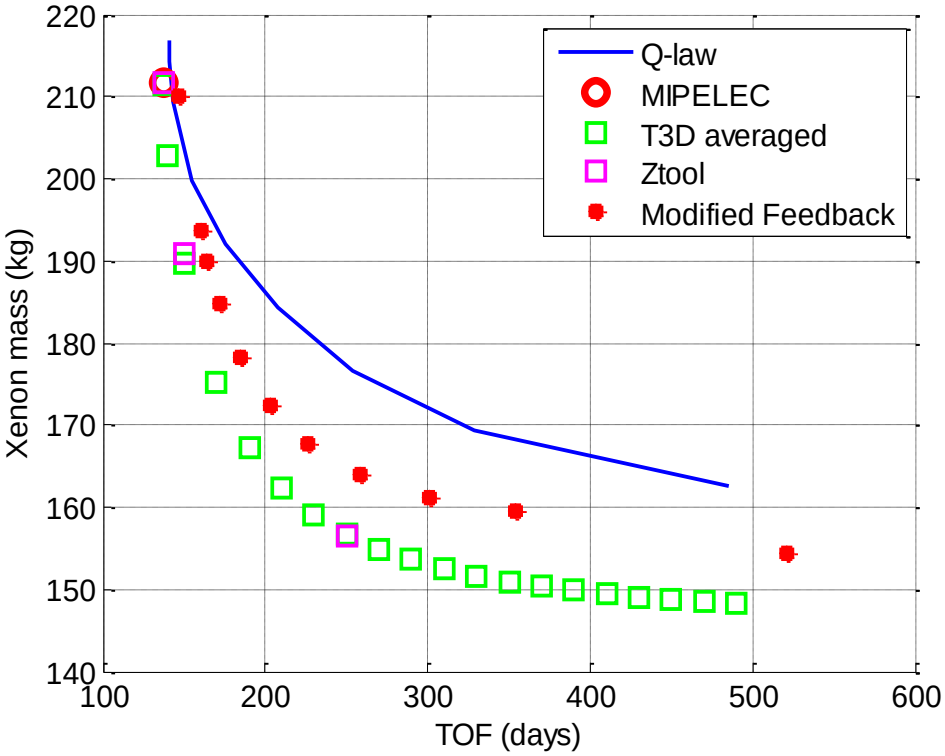

Figure 5. Fuel mass consumption vs. time-of-flight for Case B

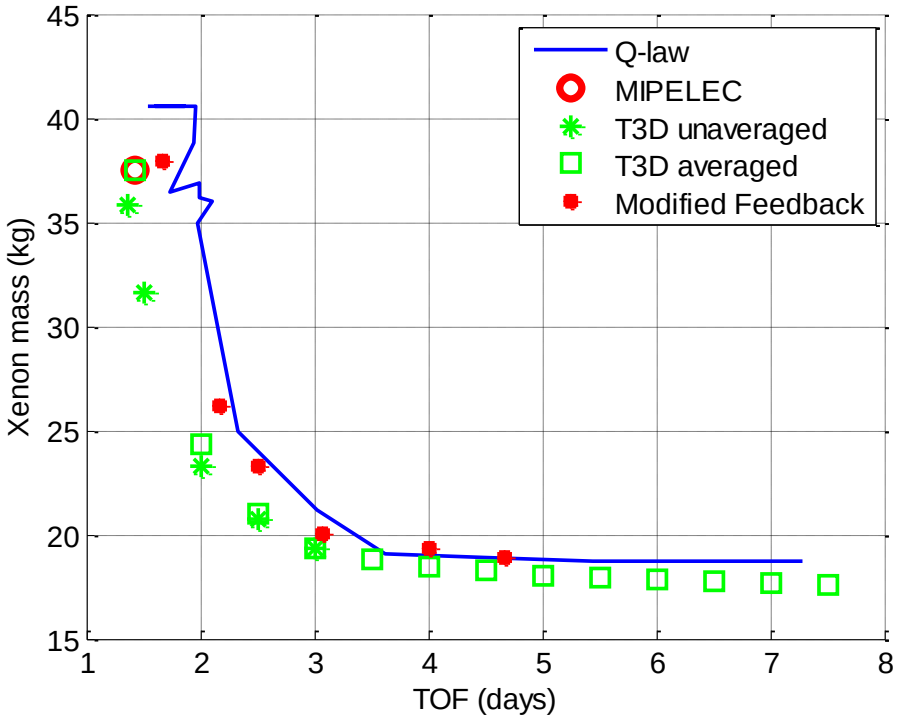

Figure 6. Fuel mass consumption vs. time-of-flight for Case C

Last is Case E, seen in Figure 7. This case involves changing all five COEs for the maneuver. As expected for such a complex case, the tool had difficulty producing an optimal solution. Case B proves that a change in semimajor axis, eccentricity, and inclination combined can be handled extremely well by the tool. In addition, running Case E for all COEs except argument of perigee produces a solution with fuel mass use values beneath the optimal curve produced by the more robust methods. This means that maneuvers including a change in the right ascension of the ascending node can also be solved using the tool with a relatively high optimality. Unfortunately, this also means that the tool is not suited to handle maneuvers with a change in the argument of perigee combined with the other orbital elements.

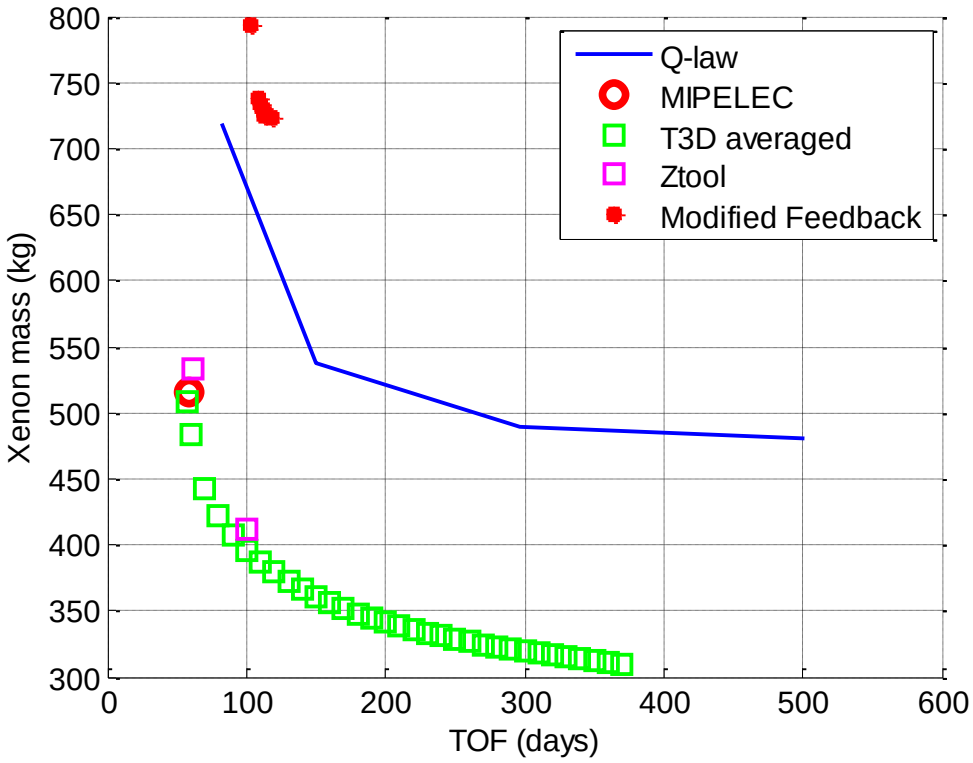

Figure 7. Fuel mass consumption vs. time-of-flight for Case E

RESULTS

Now that it has been show that the feedback control technique works for most desired cases, it can be demonstrated with certainty that the technique allows for optimizing transfers that encounter eclipse shutoff periods.

Accounting for Shutoff Periods

As mentioned earlier, in applying the efficiency weighting and threshold, average efficiency values are found looking forward over one whole orbit. The ability to do this is what allows for eclipse periods to be taken into account. With a function to find the locations in the orbit where eclipsing occurs, the eclipse locations can be assumed to have an efficiency of zero when calculating the average efficiency over the orbit. As seen comparing Figures 8a and 8b, since the eclipse is centered at perigee (the most efficient point to thrust) this results in a lower average efficiency value for the orbit than when the eclipse isn't factored in. When finding the instantane-

ous efficiency relative to the average value and comparing it to the desired efficiency threshold, this adjustment allows for thrusting at less efficient points to ensure that the trajectory is still completed.

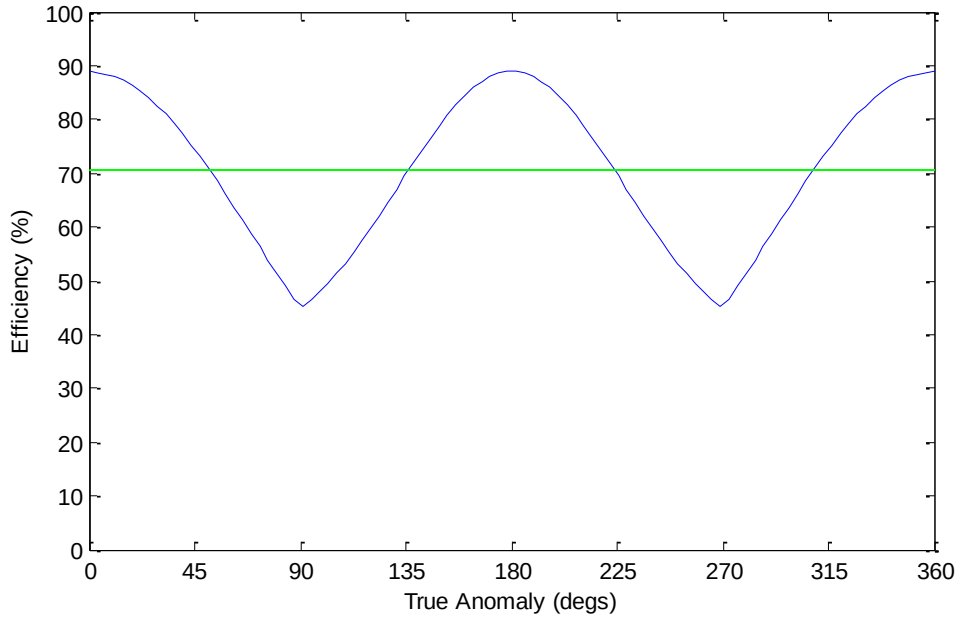

(A)

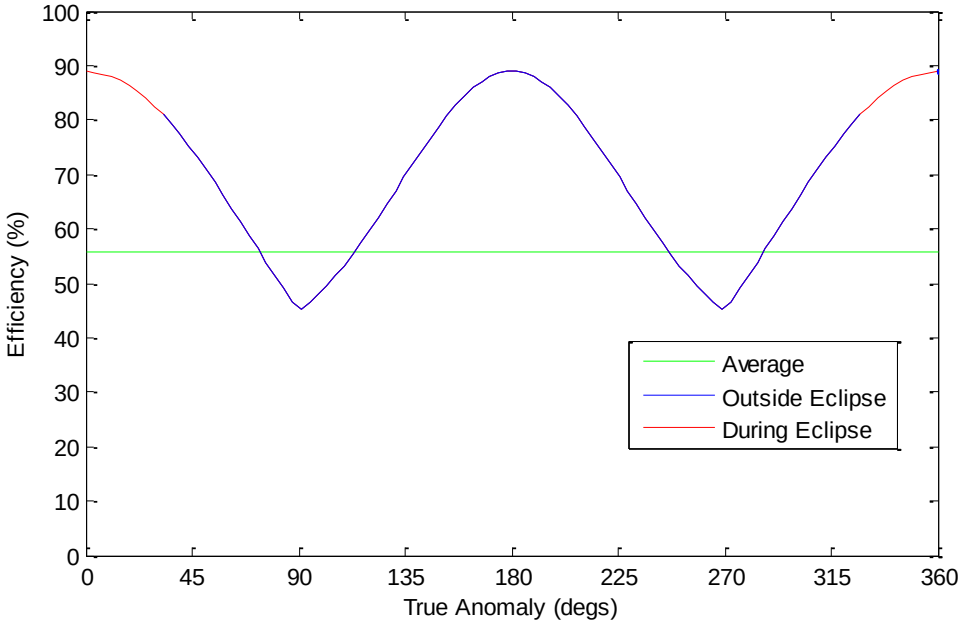

(B)

Figure 8. (A): Instantaneous and Average Efficiency Without Eclipse Periods (B): Instantaneous and Average Efficiency With Eclipse Periods

Optimizing for Eclipses

To show how this affects the optimality of the transfer, an example scenario was run with the initial and final COEs seen in Table 4.

Table 4. Initial and Final COEs for the Transfer Scenario

COE	Initial State	Desired Final State
a	16,000 km	18,000 km
e	0.5	0.4
i	0°	5°
Ω	100°	100°
ω	0°	0°

Figures 9 and 10 show this example scenario for various efficiency thresholds. In Figure 9, two scenarios are compared: optimized for eclipse periods, and including eclipse periods as unplanned outages. Looking at them closely, the results are as expected for a method that successfully optimizes for eclipse periods. As seen in the plot, not optimizing for eclipses always uses less fuel, but takes longer to complete the transfer for each given efficiency threshold. As the efficiency threshold increases, the distance between the points on the two curves increases as well, where the difference between the maneuver times increase as the fuel consumption converges. Thinking about how the eclipses affect the mass/time curve, this makes sense. Simply not thrusting during eclipses means adding maneuver time but always thrusting when its only the most efficient to do so, maintaining a low fuel mass use. When optimizing for the eclipse periods, since the efficiency threshold is compared to the new lower average efficiency value (as shown in Figure 8), thrusting is now allowed at somewhat less optimal times. This means that more fuel will be used each revolution. Since the new thrusting times are less efficient than all times spent thrusting when not optimizing for the eclipses, it takes more mass to complete the transfer. As the efficiency threshold is increased, the amount of extra time spent thrusting increases and so does the efficiency of the newly allowed thrusting region. With higher thrusting efficiencies, the fuel mass use approaches the mass use value for when not optimizing for the eclipse periods. The increased time spent thrusting each revolution decreases flight time compared to accounting for eclipse periods as unplanned shutoffs. The result is an overall higher fuel/time curve when not optimizing for eclipses, as reflected in the below plot. The differences in the two curves demonstrate how optimizing for the eclipse periods improves the accuracy of the results compared to simply not thrusting during the eclipses.

Figure 10 shows the trajectory optimized for eclipse periods again, as well as the result when eclipse periods aren't included at all. Since the eclipse occurs at perigee in this scenario (the most efficient points to thrust in the orbit), adding in the eclipse periods causes an overall increase in maneuver time and fuel consumption for most of the curve. However, the two scenarios are almost identical because optimizing for eclipses allows for additional thrusting to help counteract the shutoffs, as is the goal of optimizing for eclipse periods. Though eclipses are included in one of the scenarios, optimizing the transfer and thrusting in different places can provide a similar curve to the favorable, eclipse-free result.

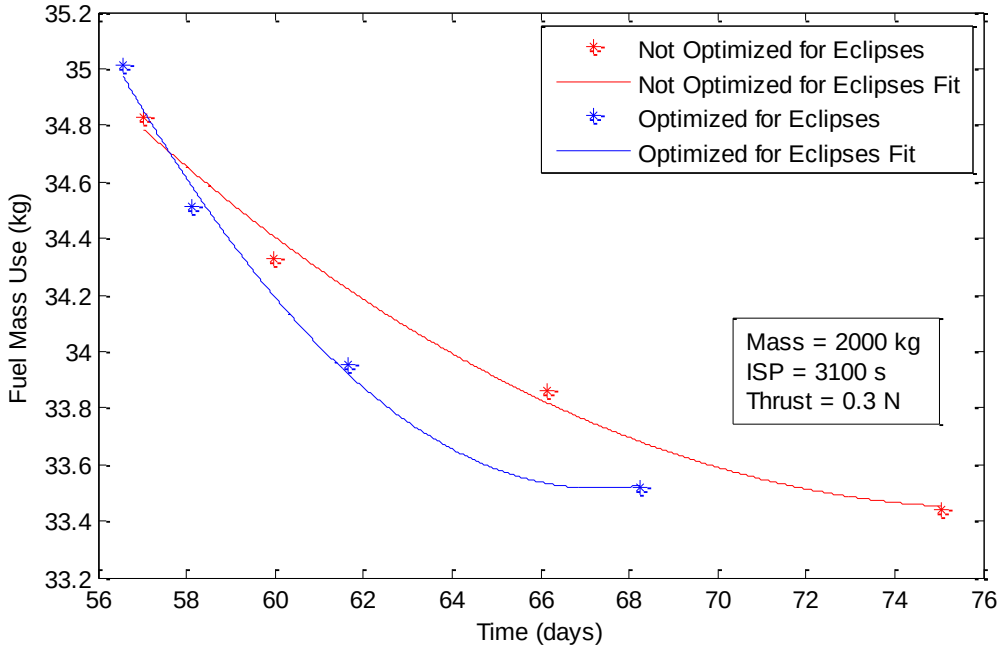

Figure 9. Maneuver Time vs. Propellant Mass Consumption Optimized and Not Optimized for Eclipse Periods

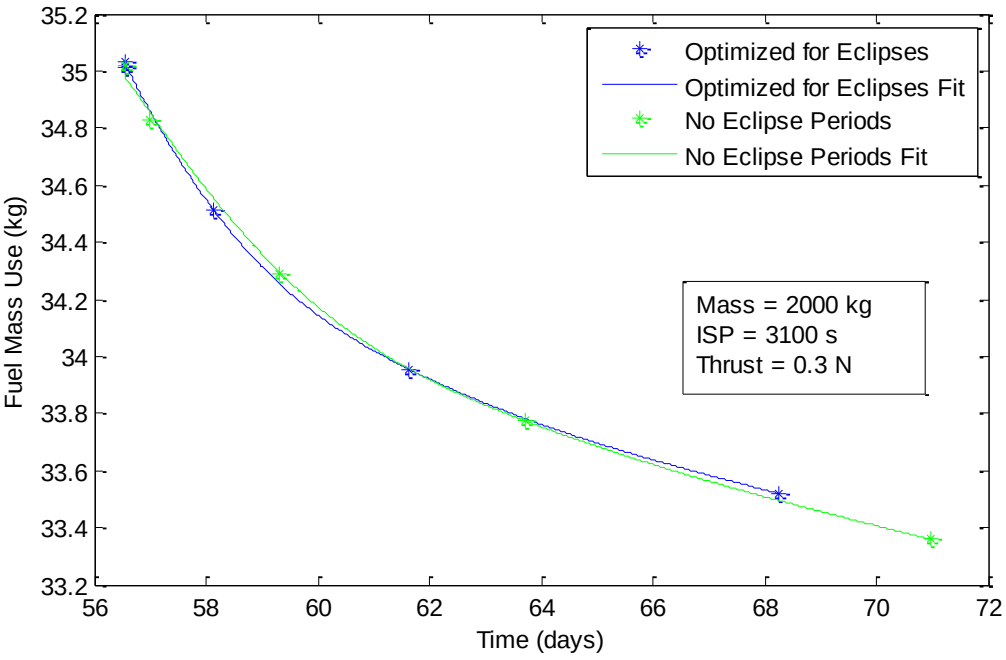

Figure 10. Maneuver Time vs. Propellant Mass Consumption Optimized for Eclipse Periods and Without Eclipse Periods

CONCLUSION

Having proven the validity of the feedback control tool created throughout this study, the results for a transfer scenario were compared for various cases, showing how the tool successfully optimizes for eclipse periods. Other tools currently in use in the aerospace industry employ various different techniques of solving for many-revolution, electric-propulsion trajectories that only allow for eclipses to be accounted for as un-planned shutoffs. It was shown that this can affect the fuel mass use vs. maneuver time curve, especially at higher efficiency thresholds. In order to best predict the performance of the mission, the eclipses need to be optimized for when solving the trajectory. The hope is that the results of this study will lead to similar techniques being employed in other, more robust tools used throughout the industry so that this can be accomplished for future missions.

ACKNOWLEDGMENTS

This research was carried out at the Jet Propulsion Laboratory, California Institute of Technology, and was sponsored by the Summer Internship Program and the National Aeronautics and Space Administration.

REFERENCES

[1] Petropolous, A.; Tarzi, Z.; Lantoine, G.; Dargent, T.; Epenoy, R., "Techniques For Designing Many-Revolution Electric-Propulsion Trajectories." AAS 14-3373

[2] Kluever, C.A., "Using Edelbaum's Method to Compute Low-Thrust Transfers with Earth-Shadow Eclipses", Journal of Guidance, Control, and Dynamics, Vol. 34, No. 1 (2011), pp. 300-303.

[3] Ruggiero, A.; Pergola, P.; Marcuccio, S.; Andrenucci, M., "Low-Thrust Maneuvers for the Efficient Correction of Orbital Elements." *32nd International Electric Propulsion Conference*, vol., no., pp.1-13, 11-15 Sept 2011.